

# Observation of scalar nuclear spin-spin coupling in van der Waals molecules

Micah P. Ledbetter,<sup>1,2,\*</sup> Giacomo Saielli,<sup>3</sup> Alessandro Bagno,<sup>4,†</sup> Nhan Tran,<sup>1</sup> and Michael V. Romalis<sup>1</sup>

<sup>1</sup>*Department of Physics, Princeton University, Princeton, New Jersey 08544, USA*

<sup>2</sup>*(present address) Department of Physics, University of California at Berkeley, Berkeley, California 94720-7300, USA*

<sup>3</sup>*Istituto CNR per la Tecnologia delle Membrane,*

*Sezione di Padova, Via Marzolo, 1 - 35131 Padova, Italy*

<sup>4</sup>*Dipartimento di Scienze Chimiche, Università di Padova, via Marzolo, 1 - 35131 Padova, Italy*

(Dated: June 6, 2021)

Scalar couplings between covalently bound nuclear spins are a ubiquitous feature in nuclear magnetic resonance (NMR) experiments, imparting valuable information to NMR spectra regarding molecular structure and conformation. Such couplings arise due to a second-order hyperfine interaction, and, in principle, the same mechanism should lead to scalar couplings between nuclear spins in unbound van der Waals complexes. Here, we report the first observation of scalar couplings between nuclei in van der Waals molecules. Our measurements are performed in a solution of hyperpolarized <sup>129</sup>Xe and pentane, using superconducting quantum interference devices to detect NMR in 10 mG fields, and are in good agreement with calculations based on density functional theory. van der Waals forces play an important role in many physical phenomena, and hence the techniques presented here may provide a new method for probing such interactions.

## Introduction

Scalar coupling between nuclear spins, characterized by an interaction of the form  $H_J = hJ\mathbf{I}_1 \cdot \mathbf{I}_2$ , where  $h$  is Planck's constant,  $J$  is the coupling constant, and  $\mathbf{I}_1$  and  $\mathbf{I}_2$  are the two spins involved, often referred to as J-coupling, is a staple feature of NMR spectroscopy.[1] J-coupling arises primarily from a second-order Fermi-contact interaction, which is generally thought to require covalent bonding between the two coupled spins. In covalent molecules, this interaction gives rise to observable splittings in NMR spectra whose pattern and separation provides important information on molecular structure and conformation. Such couplings vanish quickly upon increasing the number of intervening bonds, and couplings extending over more than 4-5 bonds are generally very weak if at all observable. As a consequence, the observation of a coupling constant is taken to be a signature of covalent bonding, and is accordingly exploited to establish molecular connectivities.

The two coupled nuclei are therefore generally assumed to belong to the same molecule. However, strictly there is no such requirement, as long as the electronic structure of the system allows for the two spins to be “connected” by a (possibly low) electron density.[2] Very long-range couplings involving <sup>19</sup>F have been known for a long time and often denoted as occurring “through space” (implying that the through-bond connectivity is too long to allow for coupling to be transmitted).[3, 4] Hereafter, we will use the term “through space” even though the spin-spin interactions involved are the same as in covalent molecules.[2] Such a situation holds also for even relatively weak hydrogen bonds (HB), and through-

HB couplings are now routinely analyzed in structural biochemistry.[5] Similarly, through-space  $J(^{13}\text{C}, ^{13}\text{C})$  or  $J(^1\text{H}, ^1\text{H})$  couplings have recently been reported for proteins whose conformation maintains a sufficiently small distance between coupled nuclei [6] and for [2,2]paracyclophanes [7]. Analysis of such couplings in molecules where the interacting spins are connected by covalent bonds require careful consideration of conformational effects [8] and coupling pathways [9] in order to assess their nature.

Scalar couplings in van der Waals molecules are expected to arise through the same mechanism as in the case of covalently bound spins. Pioneering computational work on Xe···Xe and Xe···H [10] predicted very small couplings (in the range of 10<sup>-3</sup> Hz). Further works using improved theoretical methods, both *ab initio* and based on density functional theory (DFT), have predicted couplings on the order of 10<sup>-1</sup> Hz in He<sub>2</sub>, (CH<sub>4</sub>)<sub>2</sub>, a variety of organic [8, 11–14] and xenon [15] complexes. Similar calculations have enabled accurate prediction of through-HB couplings.[5, 16]

Experimental detection of couplings in the range of 10<sup>-1</sup> Hz is feasible with conventional high-field NMR techniques. However, for unbound systems, chemical exchange and diffusion averages the effects of such coupling to very nearly zero in thermally polarized samples. Thus, despite the fundamental and practical implications of the existence of spin-spin couplings in unbound van der Waals molecules, there is no record of their experimental observation.

In this work, we report the first observation of scalar J-couplings between unbound spins in van der Waals complexes in a solution of hyperpolarized liquid Xe and pentane. The approach is based on earlier observations [17] that J-coupling in the presence of fast chemical exchange can be observed if one spin species is hyperpolarized, resulting in an average frequency shift of the other species. With this technique, the strength of proton NMR signal

\*Electronic address: ledbetter@berkeley.edu

†Electronic address: alessandro.bagno@unipd.it

is enhanced by a factor of  $10^6$  by SPINOE with hyperpolarized  $^{129}\text{Xe}$ . [18, 19] The measured value of J-coupling is in good agreement with density functional calculations averaged over an ensemble of spins simulating the bulk liquid phase. Van der Waals forces play an important role in many physical phenomena, and hence the ability to detect scalar couplings due to such forces may prove extremely valuable. For example, since J-couplings in unbound systems vanish quickly with distance, their detection and understanding would provide a spatial restraint akin to the nuclear Overhauser effect.

## Results and Discussion

Consider a system of two different spins, 1 (pentane protons) and 2 ( $^{129}\text{Xe}$  nuclei). The Zeeman contribution to the proton Hamiltonian in the presence of a magnetic field  $\mathbf{B} = B_z \hat{\mathbf{z}}$  is  $H_Z = -\hbar\gamma_1 \mathbf{I}_1 \cdot \mathbf{B}_0$ , where  $\gamma_1$  is the proton gyromagnetic ratio. In the presence of rapid chemical exchange, the normal J-coupling Hamiltonian,  $h\mathbf{I}_1 \cdot \mathbf{I}_2$ , averages to  $H_J = h\langle J \rangle I_1 \langle I_{2z} \rangle$ , where  $\langle J \rangle$  represents the thermodynamically averaged coupling between  $^{129}\text{Xe}$  and  $^1\text{H}$  [17], and we have assumed that the xenon spin polarization is nearly parallel to the magnetic field (note that  $J$  is given in Hz here). The Larmor precession frequency of protons (assumed to be positive) is thus  $\nu_1 = (\gamma_1/2\pi)B_z + \Delta\nu_1$ , where

$$\Delta\nu_1 = -\langle J \rangle \langle I_{2z} \rangle \quad (1)$$

and the minus sign originates from the difference in the signs of the Zeeman and J-coupling Hamiltonians.  $\langle J \rangle$  is given by [17]:

$$\langle J \rangle = n_2 \int J(r) \exp(-V(r)/kT) d^3r \quad (2)$$

where  $n_2$  is the number density of spin  $I_2$ ,  $J(r)$  is a distance-dependent coupling constant, and  $V(r)$  is an interatomic potential. Equation 2 can be rearranged so as to highlight its relationship with the bulk liquid structure, characterized by a radial distribution function  $g(r)$ :

$$\langle J \rangle = n_2 \int_V 4\pi r^2 J(r) g(r) dr. \quad (3)$$

The frequency shift  $\Delta\nu_1$  is analogous to that observed in optical pumping experiments; in vapor mixtures of alkali metals and noble gases, spin polarization of the unpaired electron of the metal produces a shift in the NMR resonance of the noble gas. The shift is due to the Fermi Contact interaction between the unpaired electron of the metal and the nucleus of the noble gas, mediated by the hyperfine coupling constant. [20] For the case of two nuclear spins the frequency shift can be parameterized as

$$\Delta\nu_1 = \frac{\gamma_1}{2\pi} \kappa \frac{8\pi}{3} M_{2z}, \quad (4)$$

where  $M_{2z} = \langle I_{2z} \rangle \mu_2 n_2 / I_2$  is the magnetization of spin 2 and  $\mu_2$  is its magnetic moment ( $\mu_2 = -3.88 \times 10^{-24}$  erg/G in the case of  $^{129}\text{Xe}$  [21]).  $\kappa$  is a dimensionless parameter representing the suppression or enhancement of the classical dipole magnetic field due to Coulomb repulsion or attraction of the particles. Recalling Eq. (1) and setting  $I_2 = 1/2$ , we have

$$\langle J \rangle = -\frac{8}{3} \kappa \gamma_1 \mu_2 n_2. \quad (5)$$

**SQUID Measurements.** Our measurements are performed using hyperpolarized xenon (typical polarization is 2-3%). Despite the use of hyperpolarized  $^{129}\text{Xe}$ , frequency shifts of Eq. 1 are quite small, on the order of tens of mHz, making detection in a high field spectrometer challenging, due to the finite linewidth of resonances (either because of homogeneous or inhomogeneous broadening) and due to small magnetic field drifts. We work in a low-field (10 mG), magnetically shielded environment (see Supplementary Information, Fig. 1), where the high absolute field stability facilitates observation of such small frequency shifts. NMR signals are monitored via high  $T_c$  superconducting quantum interference devices (SQUIDs) to achieve high sensitivity at low frequencies (magnetometric sensitivity was roughly  $0.3 \text{ nG}/\sqrt{\text{Hz}}$ ). Our measurements were performed using the following protocol: 1) The spherical sample cell was filled half full of pentane, which was then degassed via three freeze-thaw cycles under vacuum, and finally held in liquid state at about  $-100^\circ\text{C}$ . 2) Hyperpolarized xenon gas was introduced into the sample cell where it condensed to liquid state to fill the remaining half of the cell. 3) Spin precession was excited by applying a  $\pi/2$  pulse to the protons via a rotating magnetic field at the proton resonance frequency. Although this pulse was off resonance for the  $^{129}\text{Xe}$  spins, it produced small excitation, tipping them into the transverse plane by about  $1^\circ$ . Proton  $T_2$  was typically about 3.2 s, while  $^{129}\text{Xe}$   $T_1$  was about 450 s, so that many ( $\approx 50$ ) proton transients could be collected for each batch of polarized xenon. Free induction decay signals for  $^1\text{H}$  and  $^{129}\text{Xe}$  nuclei are shown in Fig. 1(a), after passing the raw signal through bandpass filters centered about the Larmor precession frequencies at 39.2 and 10.8 Hz, respectively. The magnitude Fourier transform of the raw signal is shown in Fig. 1(b) where the  $^{129}\text{Xe}$  and proton resonances can be easily identified.

The signature of the desired interaction is a proton frequency shift that is linear in the xenon magnetization. There are two sources of spurious frequency shifts that need to be accounted for. We first address dipolar fields associated with a deviation of the cell from perfectly spherical geometry (primarily due to the filling port). These effects can be compensated for by acquiring data with the magnetic field oriented in three orthogonal directions. We acquired three data sets with  $\mathbf{B}_0$  oriented along each of the three directions  $x$ ,  $y$ , and  $z$ .

Figure 2(a) shows the decay of the longitudinal compo-

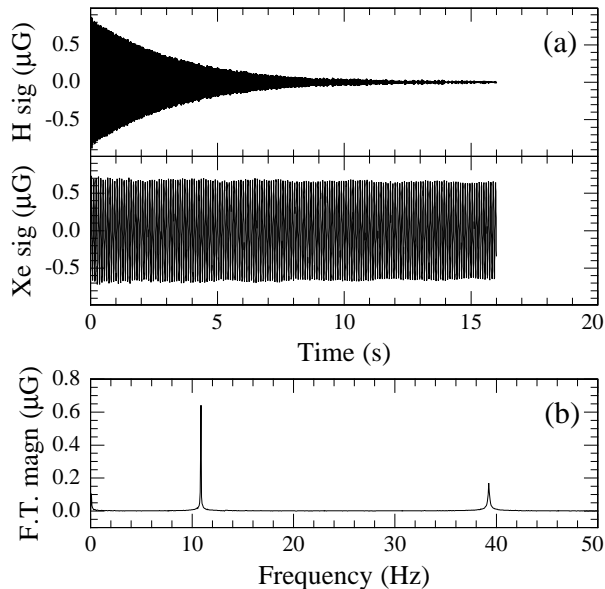


FIG. 1: Typical signals obtained in our experiment after applying a  $\pi/2$  pulse to the protons. (a) Free induction decay signals for  $^{129}\text{Xe}$  and  $^1\text{H}$  after passing the raw signal through the appropriate bandpass filters. Proton  $T_2$  was 3.2 s for these data. (b) Magnitude Fourier transform of the raw signal. Owing to the very small applied field, proton chemical shifts in pentane are unresolved, yielding a single proton line at 39.2 Hz.

ment of the magnetization, determined from the DC value of the SQUID signals. Overlying these data is a decaying exponential with time constant  $T_1 \approx 450$  s.  $^{129}\text{Xe}$  and proton resonance frequencies following each proton  $\pi/2$  pulse were determined by passing the raw signal through the appropriate bandpass filter and fitting the result to a decaying sinusoid. Figure 2(b) shows the deviation of the  $^1\text{H}$  and  $^{129}\text{Xe}$  NMR frequencies from their value in the limit of low  $^{129}\text{Xe}$  magnetization as a function of the  $^{129}\text{Xe}$  magnetization. Shown here are typical data sets for  $\mathbf{B}_0$  oriented in three different directions.

The second source of spurious frequency shifts is due to the magnetic fields associated with the pickup and feedback coils of the SQUID magnetometers. The size of this effect can be accurately determined based on the geometry of the detectors and several auxiliary spin-precession measurements (see Methods and Supplementary Information). After correcting for the effect of the SQUIDs, we verify that  $^{129}\text{Xe}$  frequency shifts vanish (scalar spin-spin couplings between  $^{129}\text{Xe}$  spins are not observable), and extract the part of the proton frequency shift that is attributed to scalar coupling with  $^{129}\text{Xe}$ .

Frequency shifts are summarized in Table I; the last row gives the net frequency shift after subtracting the shifts due to the SQUID magnetometers. The net  $^{129}\text{Xe}$  frequency shift is consistent with zero, and the average proton frequency shift per unit of magnetization along the three axes is  $\Delta\nu_1/M_{2z} = -52 \pm 11$  Hz/G, correspond-

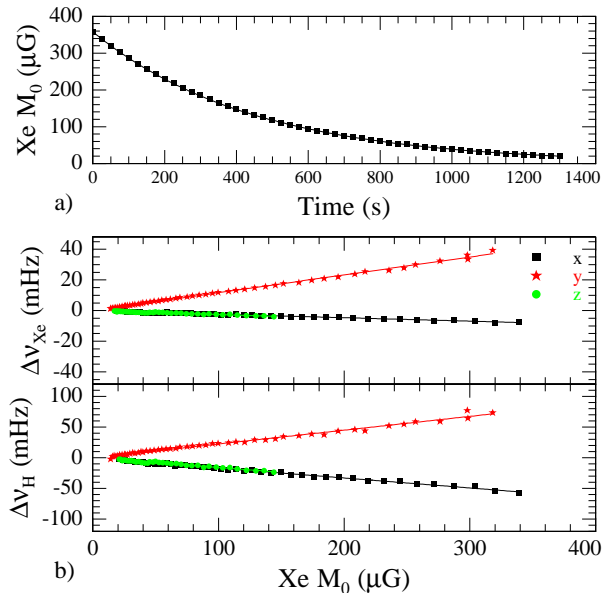


FIG. 2: (a) Decay of longitudinal component of xenon magnetization, monitored by the DC component of the SQUID signal in a typical data set. (b) Frequency shifts of  $^{129}\text{Xe}$  and  $^1\text{H}$  NMR signals for the magnetic field oriented in three orthogonal directions. The straight lines overlying the data are linear fits.

ing to  $\kappa = -0.0014 \pm 0.0003$ . The cell was half-filled with  $^{129}\text{Xe}$ , corresponding to a density  $n_2 = 7 \times 10^{21} \text{ cm}^{-3}$ . [22] Employing Eq. (5), we find  $\langle J \rangle = -2.7 \pm 0.6$  Hz. We note that accuracy and precision can be considerably improved by (a) an apparatus that overcomes some technical limitations (cell distortions, variations in cell geometry due to filling, and inaccurate measurement of the longitudinal magnetization for certain configurations of the magnetic field); (b) low- $T_c$  SQUIDs with better sensitivity ( $\approx 0.01 \text{ nG}/\sqrt{\text{Hz}}$ ) than the high- $T_c$  SQUIDs used here; (c) a higher xenon polarization than the 2-3% used in this work (polarization as high as 65% has been reported [23]).

The measured value of  $\langle J \rangle$  cannot be directly compared with DFT-calculated coupling constants for a single Xe-pentane van der Waals complex, since in the bulk phase a variety of molecular arrangements exists; thus we have combined DFT calculations with a simulation of the liquid phase as follows.

**Computational studies.** Two separate sets of calculations were carried out: First, through-space couplings were calculated with relativistic DFT methods for a series of xenon-pentane arrangements, thereby characterizing the most relevant portion of the  $^{129}\text{Xe}$ - $^1\text{H}$  coupling surface, see Figure 2 of Supplementary Information. Second, we determined the radial distribution function  $g(r)$  for the bulk liquid phase, which allows averaging of calculated coupling constants via Eq. (3). Most calculated couplings are negative and lie between  $-8$  and  $0$  Hz (a

$B_0$ direction	$\Delta\nu_1/M_{2z}$	$\Delta\nu_2/M_{2z}$	$\Delta\nu_{2,pure}/M_{2z}$
x	$-160 \pm 10$	$-21 \pm 1$	-13
y	$162 \pm 29$	$106 \pm 12$	96
z	$-170 \pm 9$	$-32 \pm 2$	-31
x+y+z	$-168 \pm 32$	$53 \pm 12$	53
SQUID shift	-12	39	39
net	$-156 \pm 32$	$14 \pm 12$	13

TABLE I: List of frequency shifts per unit of magnetization (Hz/G) for the magnetic field oriented in orthogonal directions. Errors are determined from the scatter of points over several trials, and are not given for pure xenon runs because we have collected only one data set for each direction.

few positive values are also found, as previously reported [15].

The magnitude of these couplings is consistent with the results of other computational works based on various *ab initio* and DFT theoretical methods [8, 11–15]. However, our values are larger than those reported by Salsbury and Harris for  $\text{Xe} \cdots \text{H}$  [10] by 2-3 orders of magnitude. In this regard, we note that this seminal paper [10] employed the Thomas-Fermi-Dirac functional, which is based on the uniform electron gas model. This early functional is known to suffer from neglect of electron correlation and inaccurate description of the electron density found in molecular systems [24].

The main trend of the calculated couplings features a roughly exponential decay as the distance increases from ca. 3 to 4 Å (See Supplementary Information, Figure 3). Accordingly, the couplings from the second solvation shell are mostly negligible. An orientational dependence of the coupling constants is evident from the spread of points: some relatively large couplings are predicted even when the Xe-H separation is larger than 4.0 Å. Similar anomalous distance dependences were observed in  $\text{Xe} \cdots \text{CH}_4$  [15] and in  $\text{HF} \cdots \text{CH}_4$  [11, 12] complexes. A detailed exploration of the angular dependence would probably not provide important new information, since we are only interested in the average properties of the bulk liquid phase. Calculated couplings in the range 3.0-4.3 Å were fitted to an exponential decay curve  $J(r) = ae^{-br}$ , with  $a = -2.7867 \times 10^4$  Hz,  $b = 2.719 \text{ \AA}^{-1}$ .

In Figure 3 we report the radial distribution function,  $g(r)$ , of the distance between xenon and the hydrogen atoms of pentane together with the calculated couplings and the fitting curve  $-J(r)$ . There are three groups of chemically inequivalent protons in pentane, however since chemical shifts are unresolved in our experiment, we average the radial distribution function over all hydrogen atoms. As we can see, the probability to find a Xe-H pair of atoms separated by less than 3 Å is mostly negligible, thus there is no need to carefully characterize the  $J(r)$  function for such short distances. Integration of the function of Eq. 3 with  $n_2 = 216/(31.76 \text{ \AA})^3$  (see Simulation Details below and in Supplementary Information) gives an average value  $\langle J \rangle = -3.2$  Hz, within

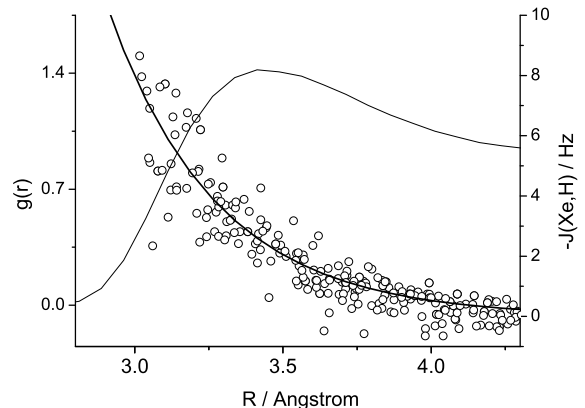


FIG. 3: (Thin line) Radial distribution function,  $g(r)$ , of the Xe-H distance averaged over all protons of pentane, right axis. (Open circles) calculated coupling constants with a negative sign for easier comparison with  $g(r)$ . (Thick line) fitting curve  $-J(r) = ae^{-br}$ , with  $a = -2.7867 \times 10^4$  Hz,  $b = 2.719 \text{ \AA}^{-1}$ , left axis.

experimental error of SQUID measurements.

It is worthwhile to stress that the averaged coupling that we have determined is somewhat different from that encountered in high-field NMR spectra, where it is usually possible to measure the coupling constants between individual spin pairs. In contrast, the coupling we have determined between pentane protons and xenon is the sum of all coupling constants between protons and all xenon atoms surrounding pentane, since each coupling produces a shift which adds to the shifts of the others. This situation is illustrated by the MD snapshot in Figure 4, where we have highlighted a single pentane molecule and the xenon atoms in the first solvation shell. Given the rapid decrease of  $J(r)$  with distance, only the closest xenon shell provides a sizable contribution to  $\langle J \rangle$ . Thus, the value of  $\langle J \rangle$  is close to that calculated at a Xe  $\cdots$  H distance of ca. 3.2 Å.

For the same reasons,  $\langle J \rangle$  depends on the density. Although the radial distribution function profile may also be density-dependent, the largest effect is simply a linear scaling of the coupling with the density of hyperpolarized xenon. Thus, in the limit of infinite dilution of pentane (cell filled with xenon), the frequency shift, and therefore  $\langle J \rangle$ , would be twice as large as in our case, where the mixture is only 50% xenon.

## Conclusions

We have reported the observation of a scalar coupling between  $^{129}\text{Xe}$  and  $^1\text{H}$  in a solution of hyperpolarized xenon and pentane. The measured value is in good agreement with calculations based on density functional theory, averaged according to the bulk liquid structure obtained by simulation. To the best of our knowledge,

## Methods

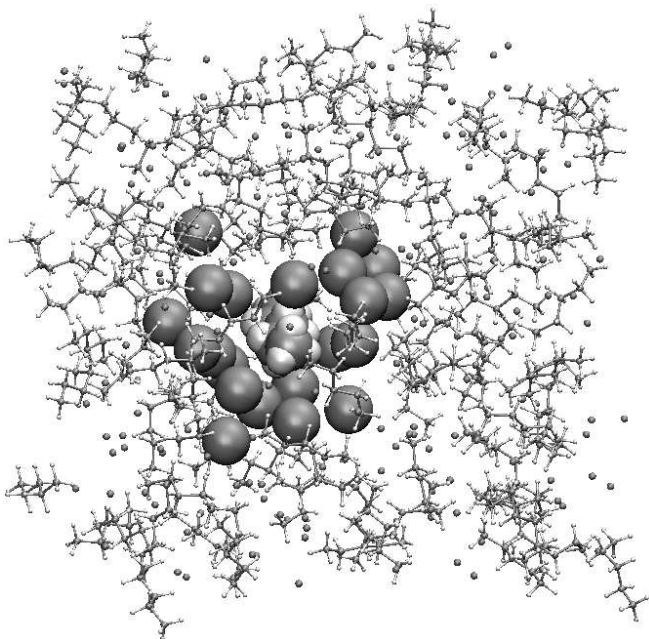


FIG. 4: Snapshot of the MD simulation box where we have highlighted a single pentane molecule and the closest xenon atoms more strongly contributing to the measured frequency shift of the pentane protons.

this is the first observation of scalar coupling mediated by van der Waals interactions in the presence of rapid chemical exchange, i.e. for “unbound” spins. Given the rapid decay of such couplings with the xenon-probe distance, their observation provides cogent information on the spatial proximity of unbound partners without complications arising from relaxation effects, as is often the case with nuclear Overhauser effects. Our measurements are facilitated by operating in very low magnetic fields, allowing us to easily vary the direction of the magnetic field  $B_0$  over three orthogonal orientations to average away the effects of dipolar fields. In principle magic angle spinning in high field may accomplish the same thing, although the necessity of vacuum tight mechanical connections to the xenon hyperpolarization system would make this challenging. Implementation of pulse sequences such as WAHUA (Wagh-Huber-Haberlein)[25], designed to mitigate the effects of dipolar fields may also enable high-field detection of such effects.

M.P.L., N.T. and M.V.R. designed and carried out SQUID experiments, analyzed the data and wrote the paper. A.B. and G.S. designed and carried out DFT calculations and MD simulations, analyzed the data and wrote the paper.

**Experimental SQUID measurements.** As typical for DC SQUID magnetometers [26], ours consist of a SQUID loop with two Josephson junctions, a superconducting pick-up coil and a normal feedback coil (inset (a), Figure S1 in the Supplementary Information). A feedback circuit controls the current in the feedback coil such that the SQUID is locked to a fixed point of its  $V(\Phi)$  curve. The current in the feedback coil serves as a measure of the applied magnetic field, but also generates small magnetic fields which can affect the precession frequency of the nuclear spins. We consider separately the AC and DC magnetic fields generated by the SQUID coils. The AC field is generated in response to the oscillating  $z$  component of the magnetization (inset (b), Fig. S1 in the Supplementary Information), and is in-phase with  $M_z$ . It can be shown from Bloch equations that the AC in-phase field will cause a shift of the  $^{129}\text{Xe}$  NMR frequency by slowly rotating the longitudinal component (parallel to  $\mathbf{B}_0$ ) of the Xe magnetization into the transverse plane. However, it does not cause an appreciable shift of the proton NMR frequency because the proton spins are tipped by approximately  $\pi/2$  relative to  $\mathbf{B}_0$ . In contrast, the DC field will affect both spin precession frequencies. It is important to take into account the fact that the SQUID feedback circuit is reset after every NMR pulse, which results in a much smaller DC field. We directly measured the AC and DC fields of the SQUIDS at the location of the spin sample by carefully measuring the dependence of the  $^{129}\text{Xe}$  NMR frequency on the applied uniform magnetic field.

**DFT calculations and molecular dynamics simulation.** Spin-spin coupling involving heavy-atom nuclei such as xenon are affected by major relativistic effects,[27] which have been dealt with by the implementation of the Zero-Order Regular Approximation (ZORA) method in the framework of DFT using the software package ADF.[28] Thus, we ran a series of calculations of the through-space  $J(^{129}\text{Xe},^1\text{H})$  coupling constants between the protons in a pentane molecule and a xenon atom, at the scalar ZORA BP86/TZ2P level, considering only the Fermi contact, diamagnetic spin-orbit, and paramagnetic spin-orbit terms.[29, 30] The position of the xenon atom was varied over a cubic grid of points, with the origin at the center of mass of the pentane molecule for a total of 1428 calculated coupling constants (see Supplementary Information, Fig. 3). The radial distribution function in the bulk liquid phase was obtained by molecular dynamics simulations, for which we used an all-atom force field (OPLS-AA) for pentane [31] and a Lennard-Jones model for xenon [32] (see the Supplementary Information for details).

## Acknowledgements

Financial support from the University of Padova (PRAT CPDA045589) is gratefully acknowledged.

M.P.L. appreciates useful discussions with Stephan Appelt, Dmitry Budker, and Alex Pines.

- 
- [1] (a) Abragam, A. *The Principles of Nuclear Magnetism* (Clarendon Press, Oxford, 1961). (b) Ernst, R. R., Bodenhausen, G. & Wokaun, A. *Principles of Nuclear Magnetic Resonance in One and Two Dimensions* (Clarendon Press, Oxford, 2004). (c) Levitt, M. H. *Spin Dynamics: Basics of Nuclear Magnetic Resonance* (Wiley, Chichester, 2008).
- [2] Bagno, A., Rastrelli, F. & Saielli, G. NMR techniques for the investigation of solvation phenomena and weak interactions. *Prog. Nucl. Magn. Reson. Spectrosc.* **47**, 41-93 (2005).
- [3] Arnold, W. D., Mao, J., Sun, H. & Oldfield, E. Computation of through-space  $^{19}\text{F}$ - $^{19}\text{F}$  scalar couplings via Density Functional Theory. *J. Am. Chem. Soc.* **122**, 12164-12168 (2000).
- [4] Dolbier, W. R. Jr. *Guide to Fluorine NMR for Organic Chemists* (Wiley, Hoboken, 2009).
- [5] Grzesiek, S., Cordier, F., Jaravine, V. & Barfield, M. Insights into biomolecular hydrogen bonds from hydrogen bond scalar couplings. *Progr. NMR Spectrosc.* **45**, 275-300 (2004).
- [6] Plevin, M. J., Bryce, D. L. & Boisbouvier, J. Direct detection of  $\text{CH}/\pi$  interactions in proteins. *Nature Chem.* **2**, 466-471 (2010).
- [7] Dračinský, M., Jansa, P., & Bouř, P. Computational and Experimental Evidence of Through-Space NMR Spectroscopy J Coupling of Hydrogen Atoms. *Chem. Eur. J.*, in press (2011). DOI: 10.1002/chem.201102272.
- [8] Bagno, A., Saielli, G. & Scorrano, G. Through-space spin-spin coupling in van der Waals dimers and  $\text{CH}/\pi$  interacting systems. An ab initio and DFT study. *Chem. Eur. J.* **8**, 2047-2056 (2002).
- [9] Malkina, O. L. & Malkin, V. G. Visualization of nuclear spin-spin coupling pathways by real-space functions. *Angew. Chem. Int. Ed. Engl.* **42**, 4335-4338 (2003).
- [10] Salsbury, F. R. & Harris, R. A. Estimation of the Fermi contact contribution to the xenon-hydrogen and xenon-xenon spin-spin coupling constants. *Mol. Phys.* **94**, 307-312 (1998).
- [11] Pecul, M. The nuclear spin-spin coupling constant in  $\text{He}_2$ . *J. Chem. Phys.* **113**, 10835-10836 (2000).
- [12] Pecul, M., Sadlej, J. & Leszczynski, J. The  $^{19}\text{F}$ - $^1\text{H}$  coupling constants transmitted through covalent, hydrogen bond, and van der Waals interactions. *J. Chem. Phys.* **115**, 5498 (2001).
- [13] Pikulska, A., Kauch, M. & Pecul, M. Theoretical prediction of the spin-spin coupling constants between an axis and macrocycle of a rotaxane. *J. Phys. Chem. A* **115**, 10795 (2011).
- [14] Bagno, A., Saielli, G. & Scorrano, G. DFT calculation of intermolecular nuclear spin-spin coupling in van der Waals dimers. *Angew. Chem. Int. Ed. Engl.* **40**, 2532-2533 (2001).
- [15] Bagno, A. & Saielli, G. DFT study of the NMR properties of xenon in covalent compounds and van der Waals complexes: implications for the use of  $\text{Xe}$ -129 as a molecular probe. *Chem. Eur. J.* **9**, 1486-1495 (2003).
- [16] Bagno, A. Quantum chemical modeling of through-hydrogen bond spin-spin coupling in amides and ubiquitin. *Chem. Eur. J.* **6**, 2925-2930 (2000).
- [17] Heckman, J. J., Ledbetter, M. P. & Romalis, M. V. Enhancement of SQUID detected NMR signals with hyperpolarized liquid  $^{129}\text{Xe}$  in a 1  $\mu\text{T}$  magnetic field. *Phys. Rev. Lett.* **91**, 067601 (2003).
- [18] Navon, G., Song, Y.-Q., Rõöm, T., Appelt, S., Taylor, R. E. & Pines, A. Enhancement of solution NMR and MRI with laser-polarized xenon. *Science* **271**, 1848-1851 (1996).
- [19] Fitzgerald, R. J., Sauer, K. L., & Happer, W. Cross-relaxation in laser-polarized liquid xenon. *Chem. Phys. Lett.* **284**, 87-92 (1998).
- [20] Schaefer, S. R. *et al.* Frequency shifts of the magnetic-resonance spectrum of mixtures of nuclear spin-polarized noble gases and vapors of spin-polarized alkali-metal atoms. *Phys. Rev. A* **39**, 5613 (1989).
- [21] Weast, R. C., Astle, M. J., Beyer, W. H. *CRC Handbook of chemistry and physics, 66 ed.* (CRC Press, Boca Raton, Florida 1985).
- [22] Rabinovich, V. A., Vasserman, A. A., Nedostup, V. I., Veksler, L. S., *Thermophysical properties of neon, argon, krypton, and xenon* (Springer-Verlag, New York 1988).
- [23] Ruset, I. C., Ketel, S. & Hersman, F. W. Optical pumping system design for large production of hyperpolarized  $^{129}\text{Xe}$ . *Phys. Rev. Lett.* **96**, 053002 (2006).
- [24] Cramer, C. J. *Essentials of Computational Chemistry. Theories and Models, 2nd Ed.* (Wiley, Chichester, 2004).
- [25] Waugh, J., Huber, L. M. & Häberlein, U., Approach to high resolution NMR in solids. *Phys. Rev. Lett.* **20**, 180 (1968).
- [26] Greenberg, Y. S. Application of superconducting quantum interference devices to nuclear magnetic resonance. *Rev. Mod. Phys.* **70**, 175 (1998).
- [27] Kaupp, M., Bühl, M. & Malkin, V. G. (Eds.), *Calculation of NMR and EPR parameters* (Wiley-VCH, Weinheim, 2004).
- [28] ADF 2004.01; te Velde, G. *et al.* Chemistry with ADF. *J. Comput. Chem.* **22**, 931-967 (2001).
- [29] (a) Becke, A. D. *Phys. Rev. A* **38**, 143 (1988). (b) Perdew, J. P. & Wang, Y. *Phys. Rev. B* **33**, 8822 (1986).
- [30] (a) Autschbach, J. & Ziegler, T. Nuclear spin-spin coupling constants from regular approximate relativistic density functional calculations. I. Formalism and scalar relativistic results for heavy metal compounds. *J. Chem. Phys.* **113**, 936-947 (2000). (b) Autschbach, J. & Ziegler, T. Nuclear spin-spin coupling constants from regular approximate relativistic density functional calculations. II. Spin-orbit coupling effects and anisotropies. *J. Chem. Phys.* **113**, 9410-9418 (2000).
- [31] Jorgensen, W. L., Maxwell, D. S. & Tirado-Rives, J. *J. Am. Chem. Soc.* Development and testing of the OPLS

- all-atom force field on conformational energetics and properties of organic liquids. **118**, 11225-11236 (1996).
- [32] Bonifácio, R. P., Filipe, E. J. M., McCabe, C., Costa Gomes, M. F. & Pádua, A. A. H. Predicting the solubility of xenon in n-hexane and n-perfluorohexane: a simulation and theoretical study. *Mol. Phys.* **100**, 2547-2553 (2002).